# In-situ momentum dispersion in a single crystal of $MoS_2$

J. M. Merlo and M. Hoag Carhart

*Physics and Astronomy Department,*
*Vassar College, 124 Raymond Ave. Poughkeepsie, NY, USA. 12604.*

Received 15 March 2024; accepted 18 April 2024

In this letter, we investigate the momentum dispersion in a $MoS_2$ flake as a function of the thickness in a single crystal with several height steps. The outcomes of our study rely on the utilization of near-field microscopy and an excitation field in the strong-coupling regime. The observed propagating modes have characteristics that are consistent with transverse magnetic (TM) modes, which can be attributed to the investigated thicknesses. Numerical simulations support our experimental findings and correspond with previously reported studies.

*Keywords:* 2D materials; TMDCs; near-field microscopy.

DOI: https://doi.org/10.31349/RevMexFis.70.050201

## 1. Introduction

The study of two-dimensional (2D) materials and their properties has emerged as a significant research field owing to its fascinating traits in light-matter interactions [1–3]. Graphene, a well-known two-dimensional material, has been proven to possess significant strength [4], thermal conductivity [5], and strong light-matter interactions [2]. Its advantage lies in its one-atom thickness, which is the defining characteristic of two-dimensional materials. In addition to graphene, there also exist 2D semiconductors known as transition metal dichalcogenides (TMDCs) that have shown intriguing characteristics such as direct bandgap [6] and strong light-matter interaction [7]. These features make them promising candidates for a new generation of photodetectors [8].

In recent years, molybdenum disulfide ($MoS_2$) [7] and tungsten diselenide ($WSe_2$) [9] have gained interest as TMDCs with bandgaps that fall between the visible and near-infrared range. Furthermore, these investigations have provided evidence of the propagating modes presence in $MoS_2$ and $WSe_2$ slabs. These studies have also examined the momentum dispersion in relation to the thickness of the crystals [7, 9, 10]. Regrettably, the reported outcomes of these investigations have been acquired using a set of different crystals that could potentially affect the experimental conditions.

With these in mind, we report for the first time the in-situ study of the momentum dispersion of propagating modes in a $MoS_2$ crystal with different height steps. We demonstrate that the properties of the modes are dependent on the thickness, confirming previously reported studies.

## 2. Experimental methods

### 2.1. Sample fabrication

Our sample was fabricated through deterministic transfer of 2D materials [11, 12]. To begin, we cleaved a bulk crystal of molybdenum disulfide ($MoS_2$) with Scotch tape. The tape was then applied to a clean polydimethylsiloxane (PDMS) surface to transfer the crystals. Subsequently, the crystals were identified using an optical microscope. In this study, our focus was on crystals that had a thickness ranging from 40 nm to 70 nm. The identification of these crystals was done using optical contrast [12], which is not included in this letter. After identifying the crystals, we used an additional layer of PDMS to selectively retrieve the chosen crystal. Finally, the second PDMS was placed in contact with a pristine Si wafer coated with a 100 nm layer of thermal $SiO_2$. This deposited the crystal on the substrate and the PDMS was removed. Figure 1a) depicts a schematic illustration of our fabrication method.

### 2.2. Near-field imaging

The near-field imaging was conducted with a near-field scanning optical microscope (NSOM, Nanonics Multiview 1500) in collection mode, using an apertured probe with a diameter of $\sim 300$ nm. Our instrument scanned the sample while maintaining the probe in a fixed position. In this study, we employed 1024 data points in the horizontal axis and 597 data points in the vertical axis, resulting in a resolution of approximately 37 nanometers. Our device, as is usual in near-field microscopy, has the ability to record both the topography of the sample and the near-field interactions simultaneously [13]. Through this, we were able to correlate the near-field intensity and the topography of the sample. A laser with a wavelength of 660 nm was used to illuminate the sample. The laser was focused to a spot size of $\sim 15$ $\mu$m, which was centered at the tip of the near-field probe. The sample was illuminated by the laser at an angle of 42 degrees with respect to the normal of the sample surface. Figure 1b) depicts a schematic representation of the experimental setup. We have deliberately chosen the 660 nm wavelength to ensure that we are operating in the strong-coupling regime [7]. However, this wavelength is sufficiently distant from the A-exciton of $MoS_2$ ($\sim 682$ nm) in order to facilitate the propagation of the excited modes.

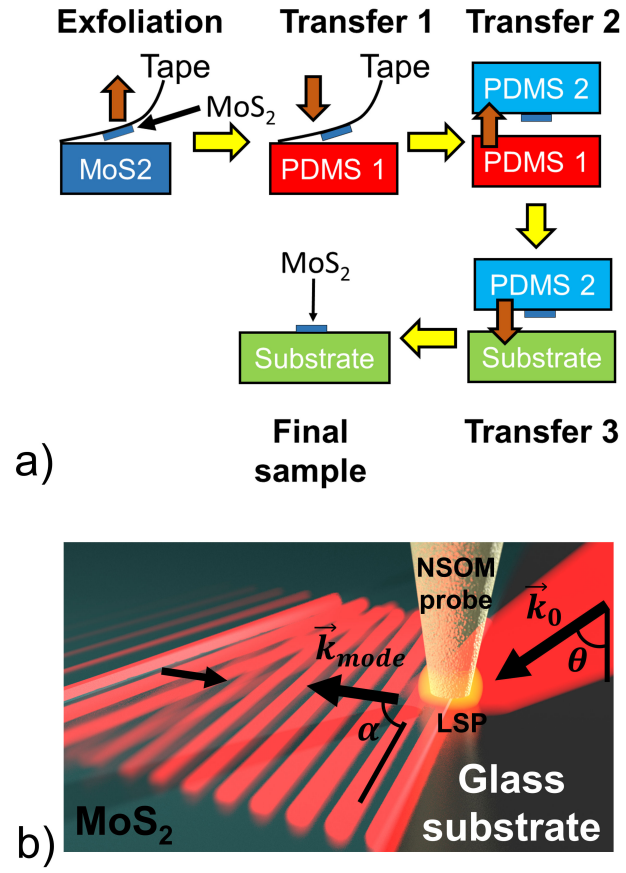


FIGURE 1. a) Illustration of the fabrication process, see main text for details. b) Schematic view of the experimental setup.

## 3. Results

### 3.1. Near-field intensity

Figure 2a) displays the topography of the crystal being examined. This crystal had several terraces of different heights. The areas of interest have been delineated by dashed lines and labeled with numbers ranging from 1 to 4 for easier identification. The heights of regions 1-4 were 40 nm, 44 nm, 54 nm, and 67 nm, respectively.

In every instance, we found an uncertainty of $\sim$ 1 nm in the height measurements. The central region in Fig. 1a), which appears to be the darkest region, was a result of an artifact caused by the piezoelectric displacement of our instrument. We are confident this was an artifact because the glass surface exhibited a flat topography with a roughness of $\sim$ 2 nm. Nevertheless, we refrained from making any additional improvements to the image due to the fact that they resulted in other, more prominent artifacts, increasing the height uncertainty.

The near-field intensity of the scan was obtained at the same time as the topography displayed in Fig. 2a), and it is depicted in Fig. 2b). We observed that the intensity image had a constant background due to the large illumination spot, as seen in the inset of Fig. 2b). To enhance the visibility of the fringes in the crystal, we implemented a Hamming filtering with a radius of 1.6 $\mu$m$^{-1}$ to remove the low spatial frequencies. The outcome is displayed in Fig. 2b). It is important to note that the fringes observed in areas 1 to 4 in Fig. 2b) were associated with propagating modes in the $MoS_2$ crystal.

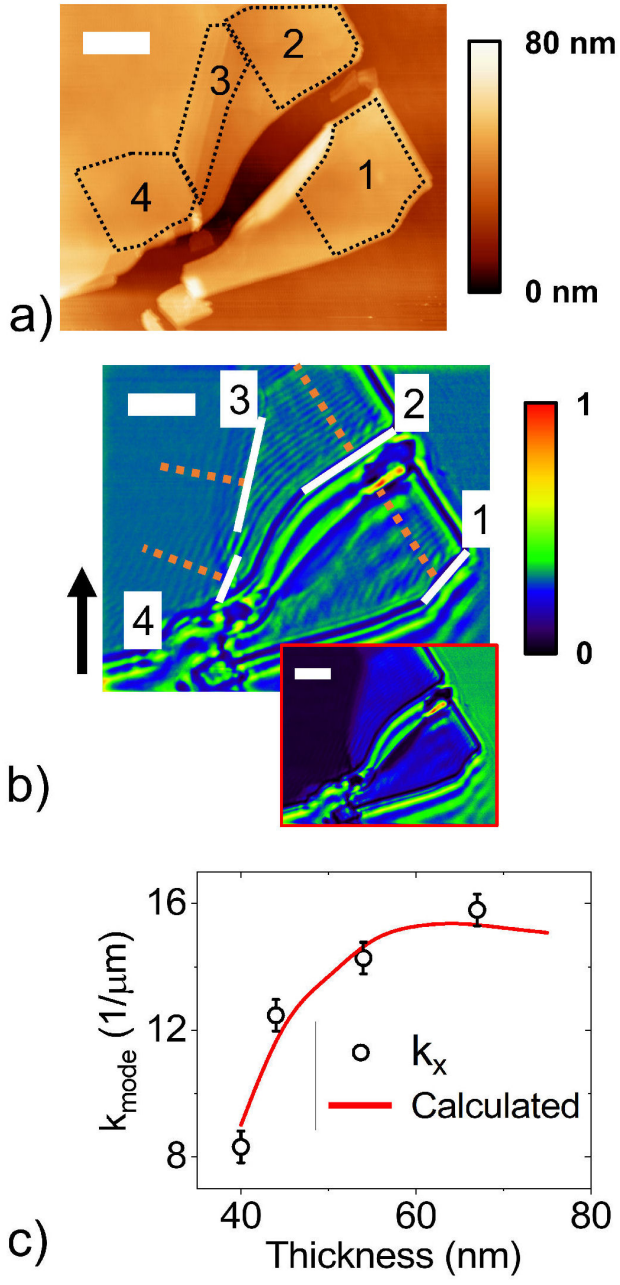


FIGURE 2. a) Topography of a $MoS_2$ crystal. b) Normalized near-field intensity after filtering. The white lines represent the edges of the crystal in the regions under study and the dashed lines represent the places where intensity cuts were made. The black arrow is the direction of the incoming excitation field. The inset shows the normalized intensity before filtering. In all the cases, the scale bar represents 5 $\mu$m. c) Momentum dispersion measured along the dashed lines in b). The black circles represent experimental data points and the red line is the numerically calculated dispersion.

The mechanism for the modes excitation can be explained as follows: the incident light generated a localized surface plasmon (LSP) at the aperture of the near-field probe [13]. This LSP possessed sufficient spatial momentum to activate the modes at the edges of the crystal. The modes propagated through the crystal and reflected at the opposite edges in regions 1 and 2. In contrast, in regions 3 and 4, the modes were not reflected back due to the absence of crystal edges with sufficient height.

The intensity fringes resulted from interference between the incident light from the excitation field, the reflection of the modes at the edges, and the localized surface plasmons (LSP). Based on the thicknesses studied and the properties of the $MoS_2$ crystal, we believe that the detected modes were predominantly transverse magnetic (TM) modes [7, 10]. We also want to emphasize that, based on our knowledge, this is the first work that demonstrates the distinct behavior of the excited modes in a single crystal.

### 3.2. Momentum dispersion

In order to determine the dispersion as function of the thickness of the crystal, we measured the near-field intensity along the orange dashed lines in Fig. 2b) and determined the spatial frequency, called $k_{NSOM}$, along each profile. The momentum in each region was calculated according to:

$$k_{mode} = k_{NSOM} + k_0 \cos(\alpha) \sin(\theta), \quad (1)$$

where $k_0$ and $\theta$ were the wave number and the angle of incidence of the excitation field respectively, and $\alpha$ was the angle between the in-plane component of the excitation field and the edge of the crystal in each region. In regions 1 through 4, the values of $\alpha$ were determined to be 45°, 55°, 10°, and 16° respectively. This information can be deducted by observing the black arrow and the white lines in Fig. 2b).

Figure 2c) displays the momentum dispersion that was determined using the near-field image, Fig. 2b), and Eq. (1). From Fig. 2c), it is evident that the mode experienced an increase in momentum as the thickness increased. This is a result of the TM character of the mode in 2D materials stimulated by near-field probes [7, 9, 10]. The error bars represent the standard deviation of the measured momentum in three different places in the studied regions 1 through 4.

In order to confirm our experimental findings, we developed a numerical model using the finite element method (FEM) to analyze the supported modes in our sample. Our model solved the equation $\mu\nabla \times (\nabla \times \vec{E}) - k^2(\epsilon - i\sigma/\omega\epsilon_0)\vec{E} = 0$ to find the out-of-plane propagation constant $k$, where $\mu$, $\epsilon$, and $\sigma$ were the permeability, permittivity, and conductivity of the material under analysis respectively, while $\epsilon_0$ was the permittivity of vacuum. $\omega$ was the angular frequency and $\vec{E}$ the electric field.

Our numerical model accurately replicated the properties of our sample, specifically, the same materials and thicknesses. The outcome is depicted as the red line in Fig. 2c). Our model demonstrated a good correlation with our experimental results. Moreover, it accurately predicted the bending at ∼67 nm thickness and the significant decrease in momentum below 50 nm thickness, which can be attributed to the transverse magnetic (TM) nature of the modes, shown in previous reports [7,10].

## 4. Conclusions

In summary, we investigated the influence of thickness on the mode characteristics in a single $MoS_2$ crystal through the use of near-field microscopy. The observed momentum dispersion has shown the transverse magnetic nature of the excited modes, indicating a significant drop below a thickness of 50 nm and a bend at 67 nm. Our experimental results are further validated by numerical simulations, which are consistent with previously published findings.


1. L. Huang *et al.*, Enhanced light-matter interaction in twodimensional transition metal dichalcogenides, *Rep. Prog. Phys.* **85** (2022) 046401, https://doi.org/10.1088/1361-6633/ac45f9
2. F. H. L. Koppens, D. E. Chang, and F. J. G. de Abajo, Graphene Plasmonics: A Platform for Strong Light Matter Interactions, *Nano Lett.* **11** (2011) 3370, https://dx.doi.org/10.1021/nl201771h
3. J. Pei, J. Yang, and Y. Lu, Elastic and Inelastic Light-Matter Interactions in 2D Materials, *IEEE J. Quantum Electron.* **23** (2017) 9000208, https://doi.org/10.1109/JSTQE.2016.2574599
4. X. Zhao *et al.*, The Strength of Mechanically-Exfoliated Monolayer Graphene Deformed on a Rigid Polymer Substrate, *Nanoscale* **11** (2019) 14339, https://doi.org/10.1039/C9NR04720D
5. A. A. Balandin *et al.*, Superior Thermal Conductivity of Single-Layer Graphene, *Nanoletters* **8** (2008) 902, https://doi.org/10.1021/nl0731872
6. C. Lin *et al.*, Direct Band Gap in Multilayer Transition Metal Dichalcogenide Nanoscrolls with Enhanced Photoluminescence, *ACS Materials Lett.* **4** (2022) 1547, https://doi.org/10.1021/acsmaterialslett.2c00162
7. P. Kusch *et al.*, Strong light-matter coupling in MoS2, *Phys. Rev. B* **103** (2021) 235409, https://doi.org/10.1103/PhysRevB.103.235409
8. O. Lopez-Sanchez *et al.*, Ultrasensitive Photodetectors Based on Monolayer MoS2, *Nat. Nanotech.* **8** (2013) 497, https://doi.org/10.1038/NNANO.2013.100
9. Z. Fei *et al.*, *et al.*, Nano-Optical Imaging of WSe2Waveguide Modes Eevealing Light-Exciton Interactions, *Phys. Rev.*

*B* **94** (2016) 081402, https://doi.org/10.1103/PhysRevB.94.081402.

10. D. Hu *et al*., Probing optical anisotropy of nanometerthin van der waals microcrystals by near-field imaging, *Phys. Rev. B* **8** (2017) 081402, https://doi.org/110.1038/s41467-017-01580-7
11. Q. Zhao *et al*., An inexpensive system for the deterministic transfer of 2D materials, *J. Phys.: Mater* **3** (2020) 016001, https://doi.org/10.1103/PhysRevB.94.081402.
12. R. Frisenda *et al*., Recent progress in the assembly of nanodevices and van der Waals heterostructures by deterministic placement of 2D materials, *Chem. Soc. Rev*. **43** (2018) 53, https://doi.org/10.1039/c7cs00556c
13. J. M. Merlo, C. Rhoads, and M. H. Carhart, Anisotropic Generation and Detection of Surface Plasmon Polaritons Using Near-Field Apertured Probes, *IEEE Phot. Jour.* **15** (2023) 4800405, https://doi.org/10.1109/JPHOT.2023.3309890